BIOCHEMISTRY
including biophysical chemistry & molecular biology
Article

*Biochemistry* **2011,** *50,* 899–909 899
DOI: 10.1021/bi1018286

# Coupling of Oligomerization and Nucleotide Binding in the AAA+ Chaperone ClpB[†]

Nicolas D. Werbeck, Cathleen Zeymer, Julian N. Kellner, and Jochen Reinstein*

*Department of Biomolecular Mechanisms, Max Planck Institute for Medical Research, Jahnstrasse 29, 69120 Heidelberg, Germany*

*Received November 15, 2010; Revised Manuscript Received December 22, 2010*

ABSTRACT: Members of the family of ATPases associated with various cellular activities (AAA+) typically form homohexameric ring complexes and are able to remodel their substrates, such as misfolded proteins or protein−protein complexes, in an ATP-driven process. The molecular mechanism by which ATP hydrolysis is coordinated within the multimeric complex and the energy is converted into molecular motions, however, is poorly understood. This is partly due to the fact that the oligomers formed by AAA+ proteins represent a highly complex system and analysis depends on simplification and prior knowledge. Here, we present nucleotide binding and oligomer assembly kinetics of the AAA+ protein ClpB, a molecular chaperone that is able to disaggregate protein aggregates in concert with the DnaK chaperone system. ClpB bears two AAA+ domains (NBD1 and NBD2) on one subunit and forms homohexameric ring complexes. In order to dissect individual mechanistic steps, we made use of a reconstituted system based on two individual constructs bearing either the N-terminal (NBD1) or the C-terminal AAA+ domain (NBD2). In contrast to the C-terminal construct, the N-terminal construct does not bind the fluorescent nucleotide MANT-dADP in isolation. However, sequential mixing experiments suggest that NBD1 obtains nucleotide binding competence when incorporated into an oligomeric complex. These findings support a model in which nucleotide binding to NBD1 is dependent on and regulated by trans-acting elements from neighboring subunits, either by direct interaction with the nucleotide or by stabilization of a nucleotide binding-competent state. In this way, they provide a basis for intersubunit communication within the functional ClpB complex.

Hsp104 and its bacterial homologue ClpB[1] are molecular chaperones that have been shown to increase thermotolerance of their respective organisms by disaggregating protein aggregates (*1*, *2*) in concert with the Hsp70 chaperone system (*3*, *4*). Both Hsp104 and ClpB are members of the family of "ATPases associated with various cellular activities" (AAA+), which is a class of enzymes involved in a diverse set of cellular actions including protein quality control, DNA replication, and membrane fusion (*5*, *6*). Many AAA+ proteins assemble into multimeric complexes, mostly hexameric ring-like structures, which are believed to be their active units. Despite their various roles in the cell, a common mechanistic feature of AAA+ proteins is the ability to convert the energy of ATP hydrolysis into molecular motions that remodel their substrate (*7*). According to the number of AAA+ domains on a polypeptide chain, AAA+ proteins can be grouped into class I (two AAA+ domains) and class II (one AAA+ domain) (*8*). Hsp104 and ClpB bear two AAA+ domains on one subunit and are therefore members of class I AAA+ proteins. They form homohexameric rings, which results in 12 potential active sites on one functional complex (*9*, *10*). ClpB/Hsp104-dependent protein disaggregation is coupled to the hydrolysis of ATP. Several studies on ClpB and Hsp104 suggest a strict coordination between the two AAA+ domains on one subunit and between AAA+ domains on different subunits within the hexameric ring (*11*−*16*). Despite a wealth of biochemical data and structural information, fundamental mechanistic aspects, such as how ATP hydrolysis is coordinated within the hexameric ring and how the chemical energy of ATP hydrolysis is converted into molecular motion, remain poorly understood. A key to understanding the molecular mechanism of ATP-dependent protein disaggregation is to characterize the nucleotide binding features of the AAA+ domains, which form the basis of the nucleotide-dependent mechanism. However, detailed investigations of the nucleotide interactions are hindered by the high complexity of the system with its 12 potential active sites, which makes a quantitative characterization practically impossible without prior knowledge and simplification.

In this work, we use a model system based on reconstitution of two truncated constructs of ClpB from *Thermus thermophilus* (*17*) that represent its major domains. One N-terminal construct comprises the first AAA+ domain (NBD1) and a coiled-coil domain (the M-domain) and is therefore termed NBD1-M (Figure 1). A second construct comprises the second AAA+ domain (NBD2) and a C-terminal domain and is therefore referred to as NBD2-C (Figure 1). Both constructs do not form higher order oligomers on their own. However, when mixed together they assemble into higher order complexes that even display disaggregation activity (*17*). Nucleotide binding features of NBD2-C have been studied in detail previously, and the

[†]The project was funded by the Max Planck Society and a Ph.D. scholarship to N.D.W. from the German National Academic Foundation.

*Correspondence should be addressed to this author. Tel: ++49 (6221) 486 502. Fax: ++49 (6221) 486 585. E-mail: jochen.reinstein@mpimf-heidelberg.mpg.de.

[1]Abbreviations: AAA+, ATPases associated with various cellular activities; ClpB, caseinolytic peptidase B; NBD1, nucleotide binding domain 1; NBD2, nucleotide binding domain 2; Hsp104, heat shock protein 104; $ClpB_{T.th.}$, caseinolytic peptidase B homologue from *Thermus thermophilus*; $ClpB_{E.coli}$, caseinolytic peptidase B homologue from *Escherichia coli*; MANT-dADP, 2′-deoxy- 3′-*O*-(*N*′-methylanthraniloyl)adenosine 5'-*O*-diphosphate; MANT-ADP, 2′(3′)-*O*-(*N*′-methylanthraniloyl)-adenosine 5′-*O*-diphosphate; MANT-dATP, 2′-deoxy-3'-*O*-(*N*′-methylanthraniloyl)adenosine 5′-*O*-triphosphate; NBD2-C, construct containing NBD2 of $ClpB_{T.th.}$ and the C-terminal domain; NBD1-M, construct containing NBD1 of $ClpB_{T.th.}$ and the M-domain.


Published on Web 12/23/2010

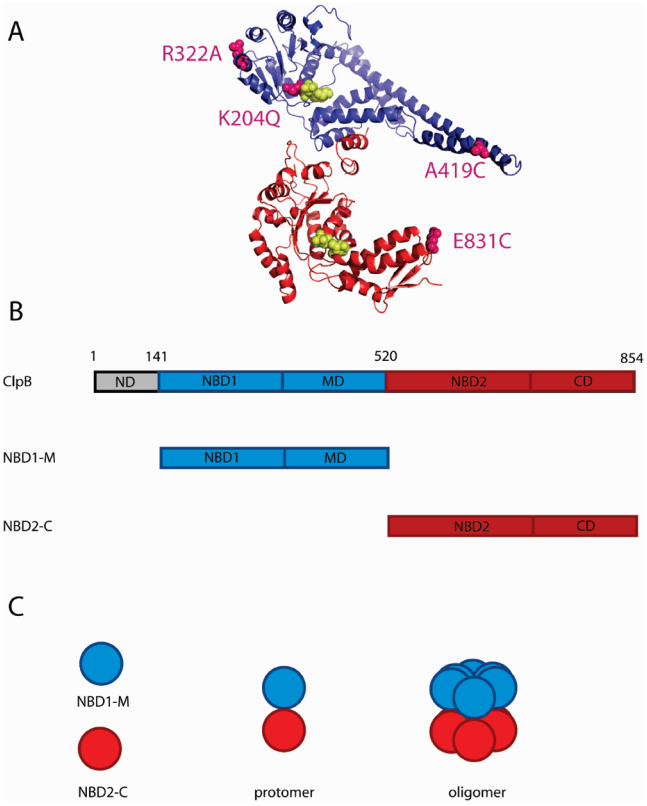


FIGURE 1: Architecture of the reconstituted ClpB system. (A) Structural model of the two constructs NBD1-M (blue) and NBD2-C (red) using the PDB file 1QVR (*9*). Bound nucleoteotides are highlighted in yellow. Mutations used in this work are indicated in magenta. The residue R322 was mutated based on a putative role in interacting with the nucleotide in trans as proposed by Tsai and co-workers (*9*). The mutation K204Q impairs nucleotide binding to NBD1 (*21*). A419C was introduced for site-specific cysteine labeling of NBD1-M; this site has been introduced successfully before (*12*). E831C has been introduced for site-specific cysteine labeling of NBD2-C. (B) Cartoon based on the primary sequence. The N-terminal domain has been shown not to be essential for chaperone activity and is therefore not included in this reconstituted system (*17*, *30*). (C) The individual constructs can assemble into ClpB protomers. Several protomers (up to six) assemble into ClpB oligomers.

fluorescent nucleotide MANT-dADP has been established for studies of nucleotide binding kinetics due to its inability to isomerize in contrast to the more commonly used MANT-ADP (*18*). These fluorescent nucleotides have the advantage of providing a very pronounced signal change upon binding, which helps to establish binding mechanisms. Once a binding mechanism has been characterized in quantitative detail, the binding kinetics of the unlabeled nucleotides ADP and ATP can be derived from competition experiments. Further, MANT-dADP and MANT-dATP bind much more tightly to NBD2-C than the unlabeled physiological nucleotides, yet still with similar discrimination between di- and triphosphates observed for the unlabeled nucleotides (ADP and ATP). This suggests that the MANT-labeled analogues serve as appropriate models for the physiological nucleotides (*18*) and represent an important tool to investigate the molecular mechanism of nucleotide binding and discrimination in the context of ATP-driven protein disaggregation.

Here, we focus on the nucleotide binding features of NBD1-M. Using a series of stopped-flow experiments, we find that NBD1-M does not bind nucleotides in isolation, yet recovers nucleotide binding competence when incorporated into an oligomeric complex. Although our applied models are simple, they are able to account for many testable predictions and suggest that in contrast to NBD2-C nucleotide binding to NBD1-M is dependent on trans-acting elements from neighboring subunits. This implication distinguishes NBD1 from NBD2 and enables the study of intersubunit communication within the ClpB complex.

## EXPERIMENTAL PROCEDURES

*Cloning and Purification*. NBD2-C and NBD1-M constructs were described previously (*17*). Mutations were introduced according to the Quikchange protocol, and positive clones were verified by DNA sequencing (Eurofins MWG, Ebersberg, Germany). Proteins were purified essentially as described before (*17*, *18*).

*Stopped-Flow Experiments*. Stopped-flow measurements were performed with a Biologic SFM-400 instrument (BioLogic Science Instruments, Claix, France) using the following delay lines: 0-MX-0 for single-mixing experiments and 0-MX-DL2 for sequential mixing experiments, where 0 stands for the absence of a delay line, MX specifies the location of a mixer (a Berger-Ball mixer), and DL2 stands for the presence of a delay line. In our experiments delay line no. 190 was used (with an intermixer volume of 220 $\mu$L).

The dead time for $t_1$, i.e., the minimal incubation time in the delay loop, for the mixing sequence was estimated to be 30 ms from a separate experiment using 2,4-dinitrophenyl acetate (DNPA) and NaOH, and this dead time was added to a given delay time $t_1$ in secondary plots. In MANT-dADP (BioLog, Bremen, Germany) binding experiments the excitation wavelength was 296 nm, and fluorescence was detected using a 400 nm cutoff filter (400FG-03-25, LOT-Oriel-group). In experiments using the Alexa-labeled variants, excitation was 478 nm and emission was monitored using a 570 nm cutoff filter (570FG-05-25, LOT-Oriel-group) for the acceptor fluorescence and a combination of 515 nm cutoff and 550 nm short-pass filter (515FG-05-25 and 550FL-07-25, respectively, LOT-Oriel-group) for donor fluorescence. In single-mixing experiments approximately three data traces were averaged; for sequential-mixing experiments single traces (at various delay times) were used for subsequent data analysis. All experiments were performed in 50 mM Tris-HCl, pH 7.5, 50 mM KCl, 5 mM $MgCl_2$, and 2 mM EDTA and at 25 °C.

*Data Analysis*. Kinetic data were analyzed using the analysis program Graphpad Prism (versions 4 and 5). Typically data were reduced to 1000 data points, and the starting point ($t = 0$) was corrected by subtracting 26 ms (the pushing time in the last mixing step). Primary kinetic data were fitted to the sum of exponential functions by a least-squares minimization procedure. In global fits, the rate constants were shared among the data set whereas all other parameters (e.g., amplitudes) were unconstrained.

*Protein Labeling*. The cysteine mutants NBD1-M A419C and NBD2-C E831C were used for specific labeling with fluorescent dyes that form FRET donor/acceptor pairs. The labeling reaction was performed according to the manufacturer's manual using the thiol-reactive dyes Alexa Fluor 546 $C_5$-maleimide and Alexa Fluor 488 $C_5$-maleimide (Invitrogen, Darmstadt, Germany) in Tris buffer (50 mM Tris-HCl, pH 7.5, 200 mM KCl, 5 mM $MgCl_2$, 2 mM EDTA). The reaction was stopped after 2 h of incubation at room temperature. Subsequently, the mixture was applied to a NAP10 column (GE Healthcare) to separate the product from free dye. The eluted sample was dialyzed into Tris buffer + 2 mM $\beta$-mercaptoethanol and washed several times to

remove residual free dye before being concentrated. Concentration and labeling efficiency were determined by UV/vis spectroscopy; the labeling efficiency was between 90% and 120%.

*Gel-Filtration Experiments*. Gel-filtration experiments were performed on a Superdex 200 column (Amersham) connected to an HPLC setup by Waters (Milford, MA) and a multiangle light scattering detector (Dawn Heleos, Wyatt, Santa Barbara, CA). The system was equilibrated to the following buffer: 50 mM Tris, pH 7.5, 50 mM KCl, 5 mM $MgCl_2$, and 2 mM EDTA (with and without the indicated concentration of nucleotide). Forty microliters of a 50 $\mu$M protein solution (NBD2-C, NBD1-M, or NBD1-M/NBD2-C complex diluted by the respective running buffer) was applied with a flow speed of 0.5 mL/min. Data analyses of the light scattering data were performed using the software ASTRA provided by the manufacturer (Wyatt). For additional reference, elution times were also compared to the elution profile of a gel-filtration standard (Bio-Rad, Catalog no. 151-1901) to calculate theoretical masses. For integration of peak areas elution profiles were corrected for baseline drifts, and peaks areas were integrated using GraphPad Prism (version 4).

*Steady-State ATPase Measurements of NBD1*. Steady-state ATP hydrolysis of NBD1 within the reconstituted complex of NBD1-M and NBD2-C was measured with a coupled colorimetric assay. The assay was performed using the NBD2-C "trap mutant" E668A, which is unable to hydrolyze ATP due to a mutation in the Walker B motif (*19*), resulting in a selective measurement of NDB1 ATPase activity in the reassembled complex. ATPase activity of NBD1 wild type and the R322A mutant were compared.

NBD1-M (12.5 $\mu$M) and NBD2-C (10 $\mu$M) were incubated at 25 °C in assay buffer (50 mM Tris-HCl, pH 7.5, 100 mM KCl, 2 mM EDTA, 2 mM DTE, 0.4 mM phosphoenolpyruvate, 0.4 mM NADH, 0.1 g/L BSA, 4 units/mL pyruvate kinase, 6 units/mL lactate dehydrogenase, and 3 mM ATP). The reaction was started by adding 7 mM $MgCl_2$. The decrease in $A_{340}$ was monitored with a JASCO V-650 spectrophotometer, and the maximal slope was used to determine the ATPase rate.

## RESULTS

*Isolated NBD1-M Does Not Bind MANT-dADP*. Previous studies indicated that the C-terminal construct of $ClpB_{T.th.}$-comprising the second AAA+ domain and the C-terminal domain (NDB2-C; see Figure 1) is able to bind nucleotides very tightly in its monomeric form. This finding suggests that all of the amino acids that are important for tight nucleotide binding are cis-acting, i.e., on the same subunit that binds the nucleotide (*18*). For NBD1 the situation is different. The separately purified construct NBD1-M, comprising NBD1 and the M-domain (see Figure 1B), binds MANT-ADP with very weak affinity only (*17*). Low nucleotide affinity was also apparent for MANT-dADP or MANT-dATP binding in stopped-flow experiments, where no change in signal upon mixing of NBD1-M with MANT-dADP or MANT-dATP was observed. To test whether this observation was due to a lack of signal rather than a lack of binding, analytical gel-filtration runs were performed in the presence of 10 $\mu$M MANT-dADP. Elution was monitored at 280 and 356 nm for protein and MANT absorption, respectively. NBD2-C, as expected, eluted with significant peaks at 280 and 356 nm, suggesting that MANT-dADP is bound, whereas NBD1-M showed almost no signal at 356 nm, confirming that NBD1-M has very low affinity to MANT-dADP (Figure 2A).

Disaggregation activity of $ClpB_{T.th.}$ requires two binding-competent nucleotide binding domains, and mutations in the Walker A motif, which impair nucleotide binding at NBD1 or NBD2, lead to loss of activity (*20*). So, the finding that separately purified NBD1-M and NBD2-C reconstitute a functional chaperone (*17*) suggests that NBD1-M could recover into a functional nucleotide binding site when incorporated into a multimeric ClpB complex including NBD2-C. When coelution experiments were performed with premixed NBD1-M and NBD2-C, the integrated area of absorption at 356 nm was ~60−70% larger than the sum of NBD1-M and NBD2-C alone (Figure 2A), suggesting that nucleotide binding to NBD1 is indeed recovered in an oligomeric complex.

The average oligomeric state of reconstituted protomers is, as for full-length $ClpB_{T.th.}$, nucleotide dependent (*17*, *20*, *21*). In the absence of nucleotides or in the presence of ATP, higher order oligomers are populated, whereas the presence of ADP triggers disassembly to lower order oligomers (Figure 2B and ref *17*). In the presence of MANT-dADP, the reconstituted system of NBD1-M and NBD2-C protomers was found to be in equilibrium between monomers and dimers (Figure 2B).

*Sequential Mixing Experiments Correlate MANT-dADP Binding to NBD1 and Complex Assembly*. To investigate how nucleotide binding to NBD1 is recovered upon formation of ClpB protomers and oligomers, we performed a series of sequential mixing experiments with a reconstituted complex of NBD1-M and NBD2-C using MANT-dADP.

Sequential mixing experiments consist of two mixing steps. In a first mixing step solutions are mixed and incubated in a delay loop, where they can react for a certain delay time ($t_1$). The reaction mixture is then mixed with another solution in the second mixing step, and this reaction can then be monitored in the cuvette. The advantage of sequential mixing experiments is that the processes that occur after the first mixing step (which happen in the delay loop) can be correlated with those that are observed after the second mixing step. In this way sequential mixing experiments could also be employed to detect processes that are spectroscopically not detectable or species that populate only transiently in the reaction.

In a first experiment 4 $\mu$M NBD2-C was mixed 1:1 with 5 $\mu$M NBD1-M and then incubated for various delay times from 130 ms to 50 s. In a second mixing step this solution was mixed 1:1 with 20 $\mu$M MANT-dADP, and binding traces were monitored by fluorescence.

The reaction system including NBD1-M, NBD2-C, MANT-dADP, and reconstituted (probably heterogeneous) oligomers cannot be described by a first-order differential equation for analysis because some of the reactions involved are not (pseudo)-first-order, in particular the assembly of the oligomeric complex. Consequently, the following analysis with exponential functions is only an approximation that describes the data traces and aims at assigning the underlying physical processes qualitatively rather than determining the microscopic rate constants of these reactions.

The data were fitted semiglobally to the sum of four exponential functions as described below (see Figure 3A). In a first hypothesis, the two fast phases were assigned to the binding of MANT-dADP (with observed rate constants ~80 and 14 $s^{-1}$) to the two different nucleotide binding domains; these phases will be referred to as $phase_1$ and $phase_2$ and their observed rate constants as $\lambda_1$ and $\lambda_2$, respectively. The slower phases ($phase_3$ and $phase_4$, with the observed rate constants $\lambda_3 = 0.5\ s^{-1}$ and $\lambda_4 = 0.12\ s^{-1}$,

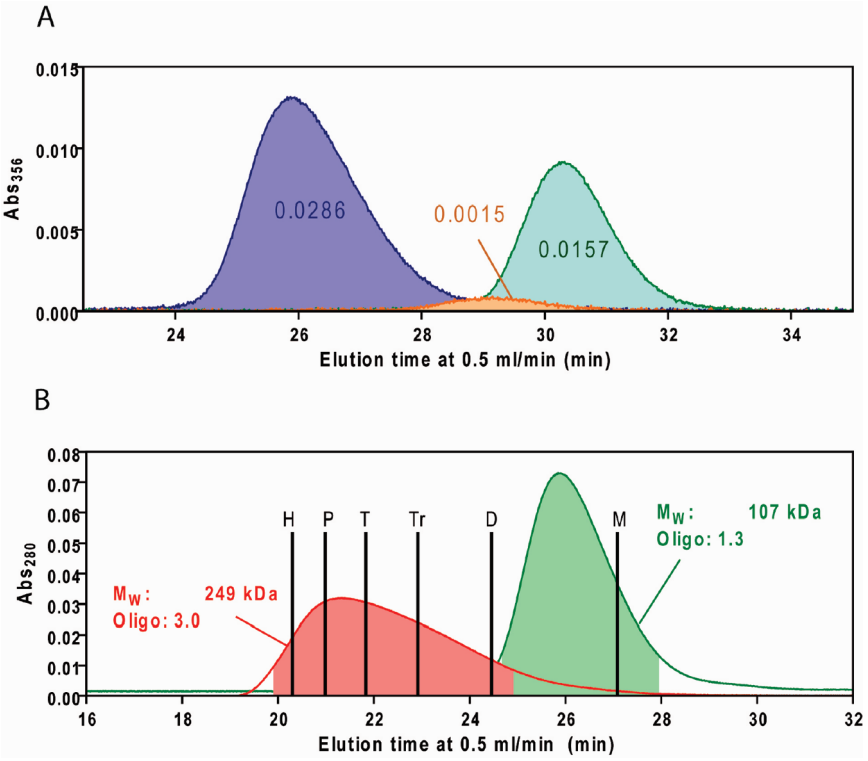


FIGURE 2: (A) Coelution of MANT-dADP with NBD1-M (orange), NBD2-C (green), and a complex of NBD1-M and NBD2-C (blue) monitored by MANT-specific absorption at 356 nm. The integrated areas for the specific peaks, which are proportional to the amount of coeluted MANT-dADP, are presented as numbers in the same color code as above. Each chromatogram represents an individual experiment. Elution profiles were corrected for baseline drifts. (B) Oligomerization of the NBD1-M/NBD2-C complex in the presence (green) and the absence (red) of 10 $\mu$M MANT-dADP. Average molecular weights as determined from multiangle light scattering data that were recorded in parallel are presented and the corresponding average oligomeric state ($M_w$ divided by 82 kDa). The part of the chromatogram used for these calculations is indicated for each individual peak (absence of MANT-dADP, red area; presence of 10 $\mu$M MANT-dADP, green area). In addition, theoretical elution times of oligomers (monomer (M), dimer (D), trimer (Tr), tetramer (T), pentamer (P), and hexamer (H)) calculated from a gel-filtration standard are indicated by black lines. Each chromatogram represents an individual experiment.

respectively) disappeared at longer delay times, which suggests that they might reflect formation of the oligomeric complex in the delay loop (Figure 3C). To facilitate comparison, this numbering of the phases and the observed rate constants will be kept consistent throughout this report. The observed rate constant of the fastest phase ($\lambda_1$) was fitted locally, as NBD2-C binds MANT-dADP in isolation and becomes only modulated upon complex formation (with $\lambda_1$ changing from ~110 to ~70 $s^{-1}$). NBD1-M does not bind MANT-dADP in isolation, and therefore $\lambda_2$, $\lambda_3$, and $\lambda_4$ were fitted globally because only the amplitudes of the corresponding phases and not their rate constants should vary significantly with delay time. We therefore describe the fit as semiglobal, because three rate constants ($\lambda_2$, $\lambda_3$, $\lambda_4$) were shared among the data sets and one rate constant ($\lambda_1$) and all other parameters were left unconstrained.

The secondary plot shows that the amplitudes of both fast phases increased with delay times (Figure 3C), suggesting that NBD1-M binds nucleotides in the assembled complex and that binding to NBD2-C is associated with higher amplitude.

To substantiate the initial assignment of the binding kinetics to NBD1 and NBD2, another sequential mixing experiment was performed. Here, 4 $\mu$M NBD2-C was preincubated with an equal amount of MANT-dADP and then mixed 1:1 with 5 $\mu$M NBD1-M in a first mixing step, and the mixture was incubated for various delay times ($t_1$). In a second mixing step this solution was mixed 1:1 with 20 $\mu$M MANT-dADP, and the binding process was monitored by increase of the fluorescence signal. If the initial assignment of the kinetic phases is correct, mainly binding to NBD1 should be observed, since NBD2, with a nanomolar $K_D$ (*18*), was already saturated with MANT-dADP, leading to a loss of phase$_1$. The primary traces could indeed be fitted globally to the sum of three exponential functions where all of the rate constants were shared among the data sets and all other parameters left unconstrained (Figure 3B). With short delay times, phase$_3$ and phase$_4$ ($\lambda_3$ = 0.5 $s^{-1}$, $\lambda_4$ = 0.1 $s^{-1}$) dominated the binding traces; as the delay time increased, the amplitudes of these phases decreased (Figure 3C), and this decrease was an exponential function of the delay time, characterized by rate constants $\lambda_{3s}$ = 0.9 $s^{-1}$ and $\lambda_{4s}$ = 0.2 $s^{-1}$ (the index "s" denotes that these rate constants have been derived from secondary plots; see Supporting Information for further explanation). The fact that $\lambda_3$ and $\lambda_{3s}$ as well as $\lambda_4$ and $\lambda_{4s}$ differ by only a factor of ~2 (which represents the difference of NBD1-M and NBD2-C concentration between delay loop and cuvette) suggests that phase$_3$ and phase$_4$ in the primary traces and in the amplitude plots monitor the same process (assuming that the protomers assemble mainly to dimers as suggested by gel filtration). Although this finding may sound trivial, there are other theoretical scenarios that could lead to a different behavior, where the observed rate constants of the primary plots and those determined from the secondary plots do not correspond. Indeed, this is the case for phase$_2$. At longer delay times phase$_2$ ($\lambda_2$ = 14 $s^{-1}$) became predominant, and the amplitudes increased with a rate constant ($\lambda_{2s}$) of 0.2 $s^{-1}$ (see Figure 3C). Here $\lambda_{2s}$ is much slower than $\lambda_2$, and it coincides with one of the observed rate constants of the assembly phases ($\lambda_{4s}$).

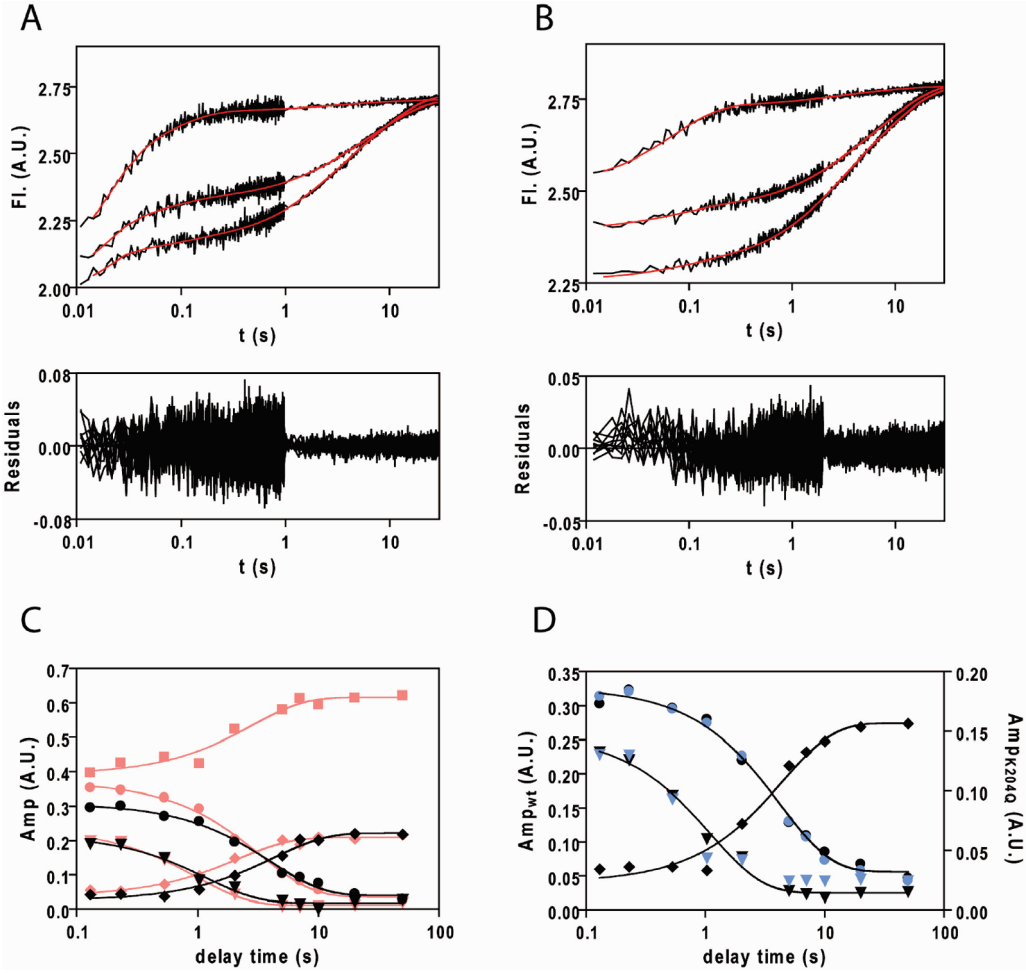


FIGURE 3: MANT-dADP binding to the reconstituted NBD1/NBD2 complex. (A) Sequential mixing experiment with a 1:1 incubation of 4 $\mu$M NBD2-C and 5 $\mu$M NBD1-M in the first mixing step followed by a 1:1 mixing with 20 $\mu$M MANT-dADP. Three example traces are given for a delay time of 0.13, 1, and 50 s (from bottom to top). The fits (see Results section for details) are shown as red lines. Residuals of all traces recorded are presented below. (B) Sequential mixing experiment with 4 $\mu$M NBD2-C preincubated with 4 $\mu$M MANT-dADP and 5 $\mu$M NBD1-M incubated 1:1 in the first mixing step followed by a 1:1 mixing with 20 $\mu$M MANT-dADP. Three example traces are given for a delay time of 0.13, 1, and 50 s (from bottom to top). The fits (see Results section for details) are shown as red lines. Residuals of all traces recorded are presented below. (C) Secondary plot of fitted amplitudes from data described in (A) and (B) versus delay time after the first mixing step. Data for the experiment that included preincubation of NBD2-C with MANT-dADP are presented in black; data without preincubation of nucleotide with NBD2-C are presented in red. The amplitudes are associated with the following rate constants as determined from the primary data: ~80 $s^{-1}$ ($\lambda_1$, red squares), 14 $s^{-1}$ ($\lambda_2$, red diamonds), 0.5 $s^{-1}$ ($\lambda_3$, red triangles), 0.1 $s^{-1}$ ($\lambda_4$, red circles), 14 $s^{-1}$ ($\lambda_2$, black diamonds), 0.5 $s^{-1}$ ($\lambda_3$, black triangles), and 0.1 $s^{-1}$ ($\lambda_4$, black circles). The amplitudes of the fastest phase (red squares) are underestimated as they approach the limits of the dead-time of this experiment. Lines represent fits to single exponential functions. (D) Secondary plot of data described in (B) (but with 20 $\mu$M final MANT-dADP) plotted in black and data taken from an equivalent experiment using NBD1-M K204Q plotted in blue. Symbols are as described in (C). The fast phase is missing for the data using the mutant, confirming that this phase can be assigned to nucleotide binding of NBD1.

The same experiment was repeated by preincubating more MANT-dADP with NBD2-C (4 $\mu$M NBD2-C and 6 $\mu$M MANT-dADP) to test whether $\lambda_2$ could be explained by a small percentage of free NBD2-C. Although we observed a slight reduction of amplitude, the results resemble the previous experimental data, suggesting that $\lambda_2$ does not arise from binding of small fractions of free NBD2-C (data not shown).

Additionally, the same experiment was performed using an NBD1-M variant bearing a mutation in the Walker A motif (K204Q). This mutant should be impaired in nucleotide binding. Consequently, if the assignment of the hypothetical NBD1-associated phase is correct, phase$_2$ should not be observed. Indeed, as shown in Figure 3D phase$_2$ is missing, suggesting that NBD1-M$_{K204Q}$ is unable to bind MANT-dADP, but the putative assembly phases, phase$_3$ and phase$_4$, are still present, suggesting that the complex assembles.

As mentioned above, the reaction system is not strictly first order or pseudo first order and can thus not be described by a system of linear ordinary differential equations with a corresponding exact solution. Moreover, the observed phases are most probably coupled, which means that they are not independent of the other reactions that take place. So the kinetic phases observed in these experiments should not be considered as reporting isolated events. However, the biochemical constraints imposed on the system (preincubation of NBD2, mutagenesis of NBD1) led to disappearance of phase$_1$ and phase$_2$, suggesting that their major contributions originate from the molecular processes assigned to these phases. In this assignment phase$_1$ represents mainly the binding of MANT-dADP to NBD2, whereas phase$_2$ represents mainly binding of MANT-dADP to NBD1.

To investigate whether $\lambda_2$ is a second-order binding rate constant, different MANT-dADP concentrations in the second mixing step (10 and 40 $\mu$M) were used. $\lambda_2$ was indeed dependent on the concentration of MANT-dADP (Figure 4A,B) whereas the rate constants associated with the slower phases ($\lambda_3$ and $\lambda_4$)

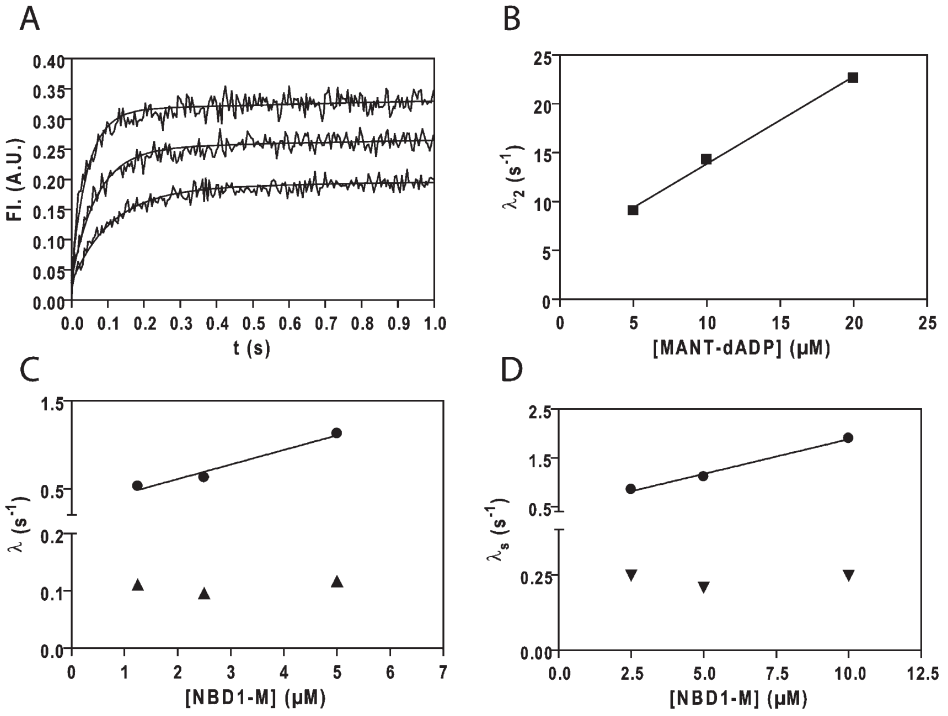


FIGURE 4: Concentration dependence of phases extracted from sequential mixing experiments. (A) Experiments as described in Figure 3B using 10, 20, and 40 $\mu$M (from bottom to top) in the last mixing step to characterize the concentration dependence of the phase that was assigned to nucleotide binding of NBD1. The final concentrations in the stopped-flow cuvette were therefore 5, 10, and 20 $\mu$M MANT-dADP, respectively, 1.25 $\mu$M NBD1-M, and 1 $\mu$M NBD2-C (MANT-dADP). Only the first 1 s of each trace with a delay time of 50 s is shown. Gray lines represent the global fits as described. To facilitate comparison of the traces, the offset was subtracted, and they all start from zero. (B) Secondary plot showing the MANT-dADP concentration dependence of the fast rate constant ($\lambda_2$, black squares). (C) Dependence of the small rate constants associated with NBD1−NBD2 assembly on the concentration of NBD1-M used in the experiments. Whereas the $\lambda_3$ (black circles) increases with increasing NBD1-M concentration, $\lambda_4$ (black triangles) remains constant. The rate constants were extracted from the global fits of the primary data. (D) Plot of the rate constants ($\lambda_{3s}$ (circles) and $\lambda_{4s}$ (triangles)) extracted from single exponential fits of the secondary amplitude plots. The amplitude of phase$_3$ (circles) decreased (as a function of delay time) more rapidly at higher NBD1-M concentrations, whereas the dependence of the amplitude of phase$_4$ (triangles) on delay time was concentration-independent. The data presented in (C) and (D) suggest that $\lambda_3$ represents the formation of the NBD1−NBD2 protomer and $\lambda_4$ represents the formation of the oligomeric complex.

were not. The kinetic $K_D$ ($k_{off}/k_{on}$) of MANT-dADP binding to NBD1 is approximately 5.5 $\mu$M, which is in good agreement with that determined for the NBD2 Walker A mutation (K601Q) of full-length ClpB (6.0 $\mu$M (*21*)). Further, the extrapolated dissociation rate constant ($k_{off}$ = 4.9 $s^{-1}$) agrees well with one of three exchange rate constants of MANT-dADP, determined by chasing prebound MANT-dADP in the reconstituted NBD1−NBD2 complex with excess unlabeled ADP ($\lambda_{ex1}$ = 4.9 $s^{-1}$, $\lambda_{ex2}$ = 0.2 $s^{-1}$, and $\lambda_{ex3}$ = 0.045 $s^{-1}$; data not shown). It is also in agreement with exchange rates determined for full-length ClpB ($\lambda_{ex1}$ = 5.8 $s^{-1}$, $\lambda_{ex2}$ = 0.76 $s^{-1}$, and $\lambda_{ex3}$ = 0.036 $s^{-1}$ (*18*)).

The picture resulting from these sequential mixing experiments is in agreement with the following model: NBD1-M does not bind MANT-dADP in isolation, and for binding of nucleotide the assembly of the NBD1−NBD2 complex is rate limiting. Therefore, slow nucleotide-independent phases, which could represent complex assembly, can be observed at short incubation times. At longer delay times, major fractions of the complex have assembled, and NBD1 binds MANT-dADP as indicated by a fast, nucleotide-dependent phase. NBD2-C, however, binds in the assembled and in the unassembled form, and therefore binding kinetics become only slightly modulated upon complex formation. In this model, two phases (phase$_3$ and phase$_4$) were assigned to the assembly process of the complex, and nucleotide binding to NBD1 coincides with the slower of these phases (phase$_4$).

*NBD1-M and NBD2-C Assemble in Two Steps*. Based on the behavior of the individual constructs, which show a reduced tendency to assemble into higher order oligomers, a simple model of NBD1-M and NBD2-C assembly can be proposed. Two processes take place for reconstitution of the ClpB complex. NBD1-M and NBD2-C bind each other to form ClpB protomers, and these protomers assemble into oligomeric complexes (Figure 1C). The gel-filtration data suggest that in the presence of MANT-dADP these oligomers are mainly dimers.

If phase$_3$ reflects the formation of the NBD1−NBD2 protomer, $\lambda_3$ should increase with higher concentration of one of the reactants (NBD1-M or NBD2-C). Thus, in order to study the assembly process in more depth, sequential mixing experiments with higher concentrations of NBD1-M were performed. Increasing the NBD1-M concentration in the first mixing step from 5 $\mu$M (before mixing) to 10 and 20 $\mu$M affected only $\lambda_3$. The slowest rate constant observed ($\lambda_4$) remained unaffected by the NBD1-M concentration used in the first mixing step (Figure 4C), and the rate constants ($\lambda_{3s}$ and $\lambda_{4s}$) extracted from the secondary amplitude plots showed the same behavior (Figure 4D).

These results are in agreement with the proposed model, in which protomer formation is assigned to phase$_3$ followed by formation of the oligomeric complex assigned to phase$_4$. The finding that $\lambda_4$ is independent of the NBD1-M concentration agrees with the fact that in the formation of the oligomeric complex the concentration of (assembled) protomer is limited by the concentration of NBD2-C and was thus constant in this series of experiments and that NBD1-M and NBD2-C form a tight protomer complex.

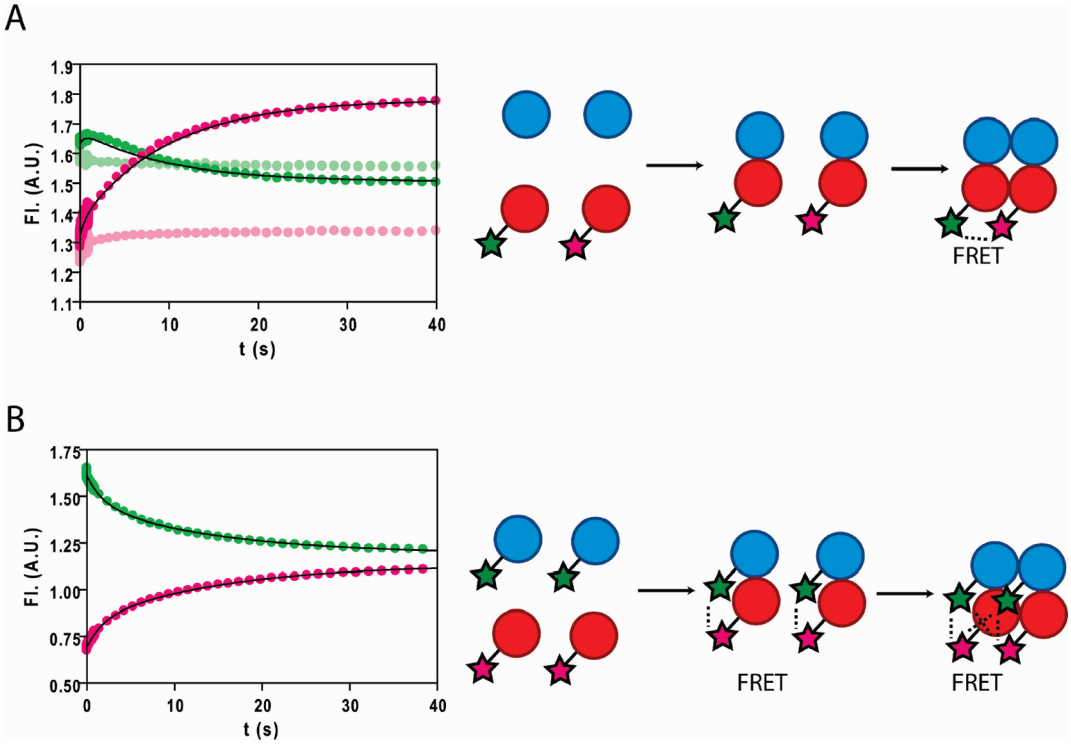


FIGURE 5: Assembly pathway monitored by fluorescence resonance energy transfer. (A) Rapid mixing of fluorescently labeled NBD2-C constructs (0.5 $\mu$M each) and unlabeled NBD1-M (1.25 $\mu$M). Donor fluorescence (Alexa-488, green) shows an initial increase followed by a slower decrease, whereas traces of acceptor fluorescence (Alexa-546, pink) only increase in fluorescence. The traces were fitted to the sum of two exponential functions with global rate constants of 1.9 and 0.1 $s^{-1}$ and local amplitudes (black lines). Traces in light green and light pink represent control experiments where the two pools of labeled NBD2-C were mixed without NBD1-M. (B) Rapid mixing of fluorescently labeled NBD2-C (Alexa-546, 1 $\mu$M) and NBD1-M (Alexa-488, 1.25 $\mu$M). Color code as in (A). Traces were fitted as in (A) to the sum of two exponential functions with the rate constants 0.5 and 0.07 $s^{-1}$. Only data in the absence of MANT-dADP are shown, but similar traces were observed in the presence of MANT-dADP (see text).

We aimed at confirming this model using a different probe and used NBD2-C and NBD1-M cysteine mutants for labeling with fluorescent dyes that form a FRET pair. The cysteine mutants were labeled in two different pools with Alexa-488 and Alexa-546 ($R_0 \sim 65$ Å) and subsequently used for reconstitution experiments. In a first experiment, two pools of labeled NBD2-C (with Alexa-488 and Alexa-546) were mixed with wild-type NBD1-M. If two NBD2-C molecules with donor (Alexa-488) and acceptor (Alexa-546) dye come into proximity, this should result in a decrease in donor fluorescence and a concomitant increase in acceptor fluorescence due to fluorescence resonance energy transfer. In stopped-flow traces a first increase of donor fluorescence was observed, followed by a pronounced decrease (Figure 5A). Although donor and acceptor signals deviated slightly from a global fit to the sum of two exponential functions with shared rate constants, the kinetic rate constants were comparable to those observed in sequential mixing experiments (with 1.9 $s^{-1}$ for the initial increase and 0.1 $s^{-1}$ for the decrease). In agreement with our model, a decrease of donor fluorescence associated with energy transfer was observed for the slower process (0.1 $s^{-1}$). Similar kinetics were observed when this experiment was conducted in the presence of MANT-dADP, with observed rate constants of 0.7 and 0.06 $s^{-1}$. In a control experiment using only donor-labeled NBD2-C a biphasic increase in fluorescence was observed with pronounced amplitude of the fast phase, suggesting that formation of the NBD1-M/NBD2-C complex is associated with a change of the environment of the fluorophore, possibly due to partial shielding, which explains the initial fluorescence increase in FRET experiments (data not shown).

A second experiment was performed by mixing Alexa-488-labeled NBD1-M and Alexa-546-labeled NBD2-C (Figure 5B). Again, two phases were observed, but here donor fluorescence decreased in both of these phases with rate constants comparable to those observed before (0.5 and 0.07 $s^{-1}$). This is again in agreement with the proposed model as mixing Alexa-labeled NBD1-M and NBD2-C constructs would bring the fluorescent donor−acceptor pair into proximity, even when they are still protomers.

In summary, our data are in agreement with an assembly of NBD1-M and NBD2-C in two steps. First, NBD1-M/NBD2-C protomers are formed followed by assembly of these protomers into oligomers in a second step. MANT-dADP binding to NBD1-M coincides with formation of oligomers, and this suggests that nucleotide binding to NBD1 depends on trans-acting elements from neighboring subunits.

*The Role of R322 as a Potential Trans-Acting Element.* The proposed model suggests that binding of nucleotides to NBD1 is dependent on trans-acting amino acids, either due to direct interaction with the nucleotide or due to stabilization of a binding-competent state of the domain. Based on structural data for full-length ClpB, a promising candidate for trans-acting interactions is arginine 322. This amino acid has been proposed to act as an arginine finger contacting the nucleotide of a neighboring subunit in a hexameric ClpB model based on cryo-EM reconstructions and the available monomeric X-ray crystal structure of ClpB (*9*). A similar arginine in *Escherichia coli* ClpB has been shown to impair oligomerization (*22*). By mutation of this arginine to alanine we aimed to answer whether arginine 322

could be the postulated trans-acting element that is crucial for binding of MANT-dADP to NBD1.

Sequential mixing experiments using NBD1-M R322A, NBD2-C, and MANT-dADP were performed as described above (Figure 6). The secondary plots derived from fitting the primary data to multiple exponentials showed a decrease in amplitudes for the phases assigned to oligomerization and MANT-dADP binding to NBD1, $phase_4$ and $phase_2$, respectively. The corresponding rate constants showed only small variations (Figure 6A). $Phase_3$, assigned to the process of protomer assembly of NBD1-M and NBD2-C, was not affected (Figure 6A). Thus, the introduced mutation R322A influences both the oligomerization phase ($phase_4$) and the nucleotide binding phase ($phase_2$) assigned to NBD1. Due to the many coupled processes in this system, amplitude information is difficult to interpret; nevertheless, it suggests that oligomerization and nucleotide binding to NBD1 are affected by the mutation.

In order to confirm the importance of R322 in the process of oligomerization, we performed gel-filtration and static light scattering experiments (as described above) with a complex of NBD1-M R322A and NBD2-C. The degree of oligomerization was reduced significantly to 2.1 in case of the R322A mutation compared to the results obtained for wild-type protein that are shown in Figure 2B.

Furthermore, stopped-flow FRET experiments were repeated using NBD1-M R322A and a mixture of the fluorescently labeled species NBD2-C Alexa-488 and NBD2-C Alexa-546. In agreement with the gel-filtration results, the amplitude of the second phase that was assigned to the oligomerization of protomers was smaller compared to the wild-type control (Figure 6C).

In the light of these results a decrease in amplitude for the phase assigned to MANT-dADP binding to NBD1 ($phase_2$) observed in the sequential mixing experiments could have two possible causes: R322 could have a direct role in stabilizing the nucleotide and the mutation therefore changes the nucleotide binding affinity, or the effect of the mutation on oligomerization could reduce the number of binding-competent NBD1 sites and therefore reduce the amplitude. In order to place the effect of R322A within these two extreme cases, the binding affinity for MANT-dADP to NBD1 R322A in the reassembled ClpB complex was estimated based on the concentration dependence of $\lambda_2$. The estimated $K_D$ for the R322A mutant differed slightly compared to the wild type, yielding a $K_D$ ($Y$-axis intercept versus slope) of ~14.1 $\mu$M for MANT-dADP binding to NBD1 in the oligomeric ClpB complex (Figure 6B) (compared to ~5.5 $\mu$M for the wild type). This modest effect of R322A on binding of MANT-dADP cannot account for the trans-acting element that we propose in this work, i.e., an element from a neighboring subunit that enables nucleotide binding at NBD1.

However, ATPase assays of the reconstituted system using NBD1-M and a hydrolysis-deficient NBD2-C mutant (E668A) show a 15-fold decrease in maximum ATPase rate of NBD1 in case of the R322A mutation compared to the wild-type control. This suggests that arginine 322 could still serve as a classical arginine finger by accelerating nucleotide hydrolysis at a neighboring NBD1.

In conclusion, the effects of the R322A mutation on the amplitude of nucleotide binding in our sequential mixing experiments are likely to reflect both: changes in oligomerization of the protomers and changes in the affinity of this mutant for MANT-dADP. However, the change in affinity due to the mutation is relatively small (a factor of ~2.5), and we therefore conclude that arginine 322 does not serve as a trans-acting element in the sense that it provides crucial binding energy for nucleotide binding to a neighboring NBD1 domain.

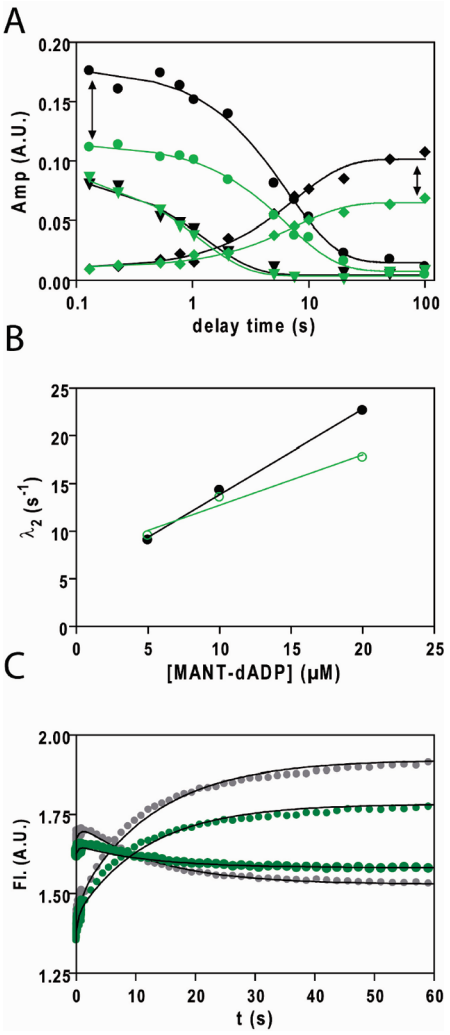


FIGURE 6: Influence of the R322A mutation on oligomerization and nucleotide binding. (A) Sequential mixing experiments as described in Figure 3B were performed using NBD1-M R322A (green symbols) and compared to equivalent experiments with NBD1-M wt (black). Symbols were used as in Figure 3C. The corresponding rate constants were obtained from the primary data fits with $\lambda_2$(R322A) = 14 $s^{-1}$, $\lambda_3$(R322A) = 0.5 $s^{-1}$, and $\lambda_4$(R322A) = 0.08 $s^{-1}$, and $\lambda_{2s}$(R322A) = 0.14 $s^{-1}$, $\lambda_{3s}$(R322A) = 0.9 $s^{-1}$, $\lambda_{4s}$(R322A) = 0.15 $s^{-1}$ for the fits of the secondary plot. (B) The concentration dependence of $\lambda_2$ for wild-type NBD1-M (black circles) and NBD1-M (R322A) (green open circles). The calculated ratios of axis intercept and slope ($k_{off}/k_{on}$) estimate a $K_D$ of ~5.5 $\mu$M for NBD1-M wt and ~14.1 $\mu$M for NBD1-M (R322A). (C) Rapid mixing FRET experiments as described in Figure 5A were performed using NBD1-M R322A and a mixture of the two fluorescently labeled NBD2-C species (Alexa-546 and Alexa-488). Donor and acceptor fluorescence are displayed as green traces; control experiments using wild-type NBD1-M are presented in gray. Traces were fitted as described in Figure 5 (A) to the sum of two exponential functions. Amplitudes corresponding to the oligomer assembly $phase_4$ were significantly reduced in case of the presence of the R322A mutation.

## DISCUSSION

The modular ClpB system presented here allows for the first time a closer analysis of the nucleotide binding properties of the individual AAA+ domains of ClpB. This revealed a complex interplay between oligomerization and nucleotide binding features,

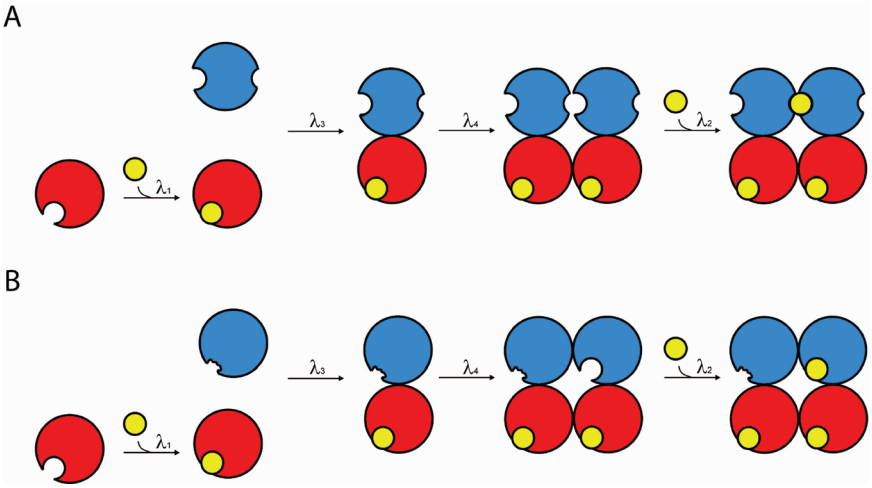


FIGURE 7: Model for the assembly of the NBD1−NBD2 complex. The stopped-flow experiments presented suggest a mechanism for the assembly of NBD1-M (blue) and NBD2-C (red). NBD2-C can bind nucleotide (represented by a yellow circle) in its monomeric form. When the two constructs are mixed, the protomer forms first; shortly afterward, the protomers form oligomeric complexes. NBD1 nucleotide binding occurs when the complex is formed, indicated by the parallel change of amplitudes of the oligomer assembly described by $\lambda_4$ and MANT-dADP binding to NBD1 described by $\lambda_2$ in secondary plots of sequential mixing experiments. The model implies that nucleotide binding to NBD1 includes either direct interaction of trans-acting residues with the nucleotide (model A) or oligomer assembly stabilizes a nucleotide binding-competent state (model B). Although this mechanism intuitively suggests a stochiometry of one bound MANT-dADP per dimer, there is so far no direct experimental evidence for this conclusion.

with implications of these features on the regulation of the ClpB ATPase cycle as discussed below.

In this reconstituted system, the two major domains, NBD1-M and NBD2-C, assemble into protomers before assembling to oligomeric complexes; these processes are described by two slow kinetic phases. Further, our data suggest that nucleotide binding to NBD1-M can be recovered when it is mixed with NBD2-C and that nucleotide binding does not depend on protomer formation; instead, it coincides with the slower assembly process, which was assigned to formation of the oligomeric, in the presence of ADP mostly dimeric, complex. A model that visualizes these interpretations and the assignments of the kinetic phase is presented in Figure 7. Thus, it appears that nucleotide binding to NBD1 involves trans-acting amino acids, either in stabilization of a binding-competent state or in direct interactions of trans-acting amino acids in nucleotide binding (Figure 7). This feature represents a difference between nucleotide binding of NBD1 and NBD2, since the latter binds nucleotides also in its monomeric form and binding is only modulated in an oligomeric complex (*18*); this difference reflects a highly coordinated reaction mechanism of ATP-driven protein disaggregation by ClpB.

If NBD1 binds ADP in its oligomerized form only, then one would expect the presence of ADP to in turn promote the assembly of the ClpB complex. However, in $ClpB_{T.th.}$ oligomerization of higher order oligomers occurs even in the absence of nucleotides, and the presence of ADP and MANT-dADP even reduces the average number of subunits within the ClpB complex (Figure 2 and refs *20* and *21*). It is possible that there are two opposing effects of ADP binding to ClpB, one that leads to disassembly, possibly through binding to NBD2, and one that supports assembly through NBD1. Gel-filtration experiments with $ClpB_{T.th.}$ conducted at 55 °C showed that a double Walker A mutation in NBD1 (K204A/T205A) does indeed not only affect ATP-induced assembly but also makes the ADP-induced disassembly more pronounced than in the wild type or the equivalent mutant of NBD2 (K601A/T602A) (*20*). The energy provided by binding of ADP to NBD1 in ClpB oligomers might counterbalance the energy released at NBD2 upon ADP-induced disassembly. Consequently, by impairment of ADP binding to NBD1, the loss of binding energy results in an even more pronounced disassembly. The data are, however, in more direct agreement with the oligomerization properties of *E. coli* ClpB ($ClpB_{E.coli}$). Here, both nucleotides promote assembly of the $ClpB_{E.coli}$ complex, although ADP does so to a smaller extent. A mutation of the NBD1 Walker A motif impairs this nucleotide-driven assembly, indicating that nucleotide binding to NBD1 favors oligomerization (*22*).

This balance of energies and their different fine-tuning in different ClpB orthologues may be the cause of opposing observations regarding the role of NBD1 and NBD2 in oligomerization of the hexameric complex. It should be noted that, in line with this model, the amplitude of $phase_4$ (representing formation of the oligomeric complex) at long delay times (50 s) in experiments described in Figure 4B increases with increasing concentrations of MANT-dADP (data not shown), suggesting that binding of the nucleotide at NBD1 could indeed favor oligomer assembly.

The data are also in agreement with the active site architecture of the ClpB relative ClpA, a AAA+ protein involved in bacterial protein degradation. In ClpA from *E. coli* the first AAA+ domain has been proposed to trigger oligomerization upon binding of ATP, based on mutational analysis (*23*) and on analysis of an ADP-bound crystal structure (*24*). In line with our model presented in Figure 7, the building blocks of ATP-induced ClpA assembly were proposed to be dimers that assemble to hexamers via a tetrameric intermediate (*25*).

The results presented here imply mechanisms of regulating nucleotide binding to NBD1. If NBD1 binds nucleotides only when embedded in an oligomeric complex, then disassembly of the complex, which was shown to be reasonably fast, should trigger nucleotide release. Although the kinetic studies so far suggest that nucleotide release from NBD1 is not rate limiting and faster than disassembly, intersubunit contacts may coordinate the ATPase cycle at NBD1 and help to impose directionality on the disaggregation process. With NBD1 and NBD2 acting as antagonists via the subunit interface, they provide the basis of a counterbalanced two-stroke engine, which avoids the trapping of

either module in an energy minimum. Further, variations in stabilizing a nucleotide binding-competent state could represent a way to modulate the ATPase cycle at NBD1. This process could involve the M-domain, which was shown to be highly flexible (*9*, *12*, *26*) and a modulator of the ClpB−ATPase cycle (*27*, *28*). Structurally the M-domain is an insertion of NBD1 at the C-terminal end (*29*), and thus it might modulate nucleotide binding and the ATPase cycle as proposed for the C-terminal domain that follows NBD2 (*18*).

To date, no high-resolution crystal structures of the hexameric ClpB complex are available, which makes it difficult to speculate on the molecular nature of the trans-acting components proposed in this study. Under these circumstances it is particularly difficult to identify potential trans-acting amino acids that interact with the nucleotide directly. On the basis of the hexameric model of *T. thermophilus* ClpB from Tsai and co-workers (*9*) we have tested the influence of an arginine that appeared to be interacting directly with the nucleotide in trans. The correlation between oligomerization of protomers and MANT-dADP binding to NBD1 underlined by experiments with NBD1-M R322A helped to confirm our interpretations of the sequential mixing data.

However, binding of MANT-dADP was only modestly affected for this mutant, indicating that arginine 322 cannot account for the full contribution in binding energy provided by elements from neighboring subunits as implied by our experiments.

The fact that steady-state ATPase activity is affected, however, is in agreement with the proposed role of an arginine finger, but given the impaired oligomerization behavior of this mutant, interpretations of our steady-state ATPase data are not straightforward.

In this work we present the use of a reconstituted system in combination with sequential mixing experiments to dissect different features of ClpB−nucleotide binding and oligomerization.

By using this model system we were able to constrain and perturb the reactions involved in nucleotide binding and oligomer assembly specifically: by preincubating with MANT-dADP, mutating individual domains selectively, or changing their concentrations. This approach facilitates a separation of coupled events and allows to describe their complex interdependence. Our model of the nucleotide binding features of the two AAA+ domains is likely to be a starting point for more elaborate models. These could include more than two different nucleotide binding sites (one for each AAA+ module) as indicated by three nucleotide exchange phases, which could result from nonidentical nucleotide binding domains within an oligomeric complex. Further, it is of great interest to investigate how nucleotide binding to one domain influences the binding features of other domains. The system presented here provides an experimental toolbox suited to tackling these questions and to learning more about the working cycle of ClpB and its nucleotide-dependent coordination.

## ACKNOWLEDGMENT

We acknowledge Jessica Eschenbach, Melanie Weisser, and Marie Rethagen for excellent technical assistance and Philipp Beinker for establishing the reconstituted system of NBD1-M and NBD2-C. We are grateful to Franz Xaver Schmid for helpful comments on this work. We thank John Wray and Tatiana Domratcheva for critical reading of the manuscript and Ilme Schlichting for continuous support.

## SUPPORTING INFORMATION AVAILABLE

A detailed explanation of the difference between rate constants derived from primary traces and those derived from secondary amplitude plots. This material is available free of charge via the Internet at http://pubs.acs.org.

## REFERENCES

1. Mogk, A., Tomoyasu, T., Goloubinoff, P., Rudiger, S., Roder, D., Langen, H., and Bukau, B. (1999) Identification of thermolabile *Escherichia coli* proteins: prevention and reversion of aggregation by DnaK and ClpB. *EMBO J. 18*, 6934–6949.
2. Sanchez, Y., and Lindquist, S. L. (1990) Hsp104 required for induced thermotolerance. *Science 248*, 1112–1115.
3. Glover, J. R., and Lindquist, S. (1998) Hsp104, Hsp70, and Hsp40: a novel chaperone system that rescues previously aggregated proteins. *Cell 94*, 73–82.
4. Motohashi, K., Watanabe, Y., Yohda, M., and Yoshida, M. (1999) Heat-inactivated proteins are rescued by the DnaK.J-GrpE set and ClpB chaperones. *Proc. Natl. Acad. Sci. U.S.A. 96*, 7184–7189.
5. Hanson, P. I., and Whiteheart, S. W. (2005) AAA+ proteins: have engine, will work. *Nat. Rev. Mol. Cell Biol. 6*, 519–529.
6. Erzberger, J. P., and Berger, J. M. (2006) Evolutionary relationships and structural mechanisms of AAA+ proteins. *Annu. Rev. Biophys. Biomol. Struct. 35*, 93–114.
7. Tucker, P. A., and Sallai, L. (2007) The AAA+ superfamily, a myriad of motions. *Curr. Opin. Struct. Biol. 17*, 641–652.
8. White, S. R., and Lauring, B. (2007) AAA+ ATPases: achieving diversity of function with conserved machinery. *Traffic 8*, 1657–1667.
9. Lee, S., Sowa, M. E., Watanabe, Y. H., Sigler, P. B., Chiu, W., Yoshida, M., and Tsai, F. T. (2003) The structure of ClpB: a molecular chaperone that rescues proteins from an aggregated state. *Cell 115*, 229–240.
10. Wendler, P., Shorter, J., Plisson, C., Cashikar, A. G., Lindquist, S., and Saibil, H. R. (2007) Atypical AAA+ subunit packing creates an expanded cavity for disaggregation by the protein-remodeling factor Hsp104. *Cell 131*, 1366–1377.
11. Schirmer, E. C., Ware, D. M., Queitsch, C., Kowal, A. S., and Lindquist, S. L. (2001) Subunit interactions influence the biochemical and biological properties of Hsp104. *Proc. Natl. Acad. Sci. U.S.A. 98*, 914–919.
12. Watanabe, Y. H., Takano, M., and Yoshida, M. (2005) ATP binding to nucleotide binding domain (NBD)1 of the ClpB chaperone induces motion of the long coiled-coil, stabilizes the hexamer, and activates NBD2. *J. Biol. Chem. 280*, 24562–24567.
13. Wendler, P., Shorter, J., Snead, D., Plisson, C., Clare, D. K., Lindquist, S., and Saibil, H. R. (2009) Motor mechanism for protein threading through Hsp104. *Mol. Cell 34*, 81–92.
14. Werbeck, N. D., Schlee, S., and Reinstein, J. (2008) Coupling and dynamics of subunits in the hexameric AAA+ chaperone ClpB. *J. Mol. Biol. 378*, 178–190.
15. del Castillo, U., Fernandez-Higuero, J. A., Perez-Acebron, S., Moro, F., and Muga, A. (2010) Nucleotide utilization requirements that render ClpB active as a chaperone. *FEBS Lett. 584*, 929–934.
16. Hoskins, J. R., Doyle, S. M., and Wickner, S. (2009) Coupling ATP utilization to protein remodeling by ClpB, a hexameric AAA+ protein, *Proc. Natl. Acad. Sci. U.S.A. 106*, 22233−22238.
17. Beinker, P., Schlee, S., Auvula, R., and Reinstein, J. (2005) Biochemical coupling of the two nucleotide binding domains of ClpB: covalent linkage is not a prerequisite for chaperone activity. *J. Biol. Chem. 280*, 37965–37973.
18. Werbeck, N. D., Kellner, J. N., Barends, T. R., and Reinstein, J. (2009) Nucleotide binding and allosteric modulation of the second AAA+ domain of ClpB probed by transient kinetic studies. *Biochemistry 48*, 7240–7250.
19. Weibezahn, J., Schlieker, C., Bukau, B., and Mogk, A. (2003) Characterization of a trap mutant of the AAA+ chaperone ClpB. *J. Biol. Chem. 278*, 32608–32617.
20. Watanabe, Y. H., Motohashi, K., and Yoshida, M. (2002) Roles of the two ATP binding sites of ClpB from *Thermus thermophilus*. *J. Biol. Chem. 277*, 5804–5809.
21. Schlee, S., Groemping, Y., Herde, P., Seidel, R., and Reinstein, J. (2001) The chaperone function of ClpB from *Thermus thermophilus* depends on allosteric interactions of its two ATP-binding sites. *J. Mol. Biol. 306*, 889–899.
22. Mogk, A., Schlieker, C., Strub, C., Rist, W., Weibezahn, J., and Bukau, B. (2003) Roles of individual domains and conserved motifs of the AAA+ chaperone ClpB in oligomerization, ATP hydrolysis, and chaperone activity. *J. Biol. Chem. 278*, 17615–17624.

23. Singh, S. K., and Maurizi, M. R. (1994) Mutational analysis demonstrates different functional roles for the two ATP-binding sites in ClpAP protease from *Escherichia coli*. *J. Biol. Chem. 269*, 29537–29545.
24. Guo, F., Maurizi, M. R., Esser, L., and Xia, D. (2002) Crystal structure of ClpA, an Hsp100 chaperone and regulator of ClpAP protease. *J. Biol. Chem. 277*, 46743–46752.
25. Kress, W., Mutschler, H., and Weber-Ban, E. (2007) Assembly pathway of an AAA+ protein: tracking ClpA and ClpAP complex formation in real time. *Biochemistry 46*, 6183–6193.
26. Zietkiewicz, S., Slusarz, M. J., Slusarz, R., Liberek, K., and Rodziewicz-Motowidlo, S. (2010) Conformational stability of the full-atom hexameric model of the ClpB chaperone from *Escherichia coli*. *Biopolymers 93*, 47–60.
27. Haslberger, T., Weibezahn, J., Zahn, R., Lee, S., Tsai, F. T., Bukau, B., and Mogk, A. (2007) M domains couple the ClpB threading motor with the DnaK chaperone activity. *Mol. Cell 25*, 247–260.
28. Watanabe, Y. H., Nakazaki, Y., Suno, R., and Yoshida, M. (2009) Stability of the two wings of the coiled-coil domain of ClpB chaperone is critical for its disaggregation activity. *Biochem. J. 421*, 71–77.
29. Barends, T. R., Werbeck, N. D., and Reinstein, J. (2010) Disaggregases in 4 dimensions, *Curr. Opin. Struct. Biol. 20*, 46−53.
30. Beinker, P., Schlee, S., Groemping, Y., Seidel, R., and Reinstein, J. (2002) The N terminus of ClpB from *Thermus thermophilus* is not essential for the chaperone activity. *J. Biol. Chem. 277*, 47160–47166.